Impaired mitochondrial transport and Parkin-independent degeneration of respiratory chain-deficient dopamine neurons in vivo

Fredrik H. Sterky[a,b], Seungmin Lee[a], Rolf Wibom[a], Lars Olson[b], and Nils-Göran Larsson[a,c,1]

Departments of [a]Laboratory Medicine and [b]Neuroscience, Karolinska Institute, SE-171 77 Stockholm, Sweden; and [c]Max Planck Institute for Biology of Ageing, D-50931 Cologne, Germany

Edited by Thomas C. Südhof, Stanford University School of Medicine, Palo Alto, CA, and approved June 30, 2011 (received for review February 28, 2011)

Mitochondrial dysfunction is heavily implicated in Parkinson disease (PD) as exemplified by the finding of an increased frequency of respiratory chain-deficient dopamine (DA) neurons in affected patients. An inherited form of PD is caused by impaired function of Parkin, an E3 ubiquitin ligase reported to translocate to defective mitochondria in vitro to facilitate their clearance. We have developed a reporter mouse to assess mitochondrial morphology in DA neurons in vivo and show here that respiratory chain deficiency leads to fragmentation of the mitochondrial network and to the formation of large cytoplasmic bodies derived from mitochondria. Surprisingly, the dysfunctional mitochondria do not recruit Parkin in vivo, and neither the clearance of defective mitochondria nor the neurodegeneration phenotype is affected by the absence of Parkin. We also show that anterograde axonal transport of mitochondria is impaired in respiratory chain-deficient DA neurons, leading to a decreased supply of mitochondria to the axonal terminals.

mitochondrial DNA | mitochondrial biogenesis | oxidative phosphorylation

Aging is a major risk factor for Parkinson disease (PD) and is associated with a decline of respiratory chain function and the accumulation of low levels of somatic mtDNA mutations (1, 2). In aging humans, it is well established that clonal expansion of these somatic mtDNA mutations causes a mosaic respiratory chain deficiency in several different cell types, such as cardiomyocytes (3), skeletal muscle cells (4), colon epithelium (5), and different types of neurons (6, 7). Studies of homogenates from aged human brains have shown that the levels of deleted mtDNA differ dramatically among regions (8, 9) with the highest levels reported in substantia nigra (SN) (9). Single-cell techniques have shown that ~1% of the dopamine (DA) neurons are respiratory chain deficient in normal aged humans because of the accumulation of mtDNA deletions (7, 10). Interestingly, the proportion of respiratory chain-deficient DA neurons is reported to be higher in persons with PD than in age-matched controls (7, 10), suggesting a possible causative role in DA neuron loss. Additional support for the hypothesis that mitochondrial dysfunction can cause PD comes from the observation that a metabolite of the toxin 1-methyl-4-phenyl-1,2,3,6-tetrahydropyridine (MPTP), which is taken up selectively by DA neurons and causes a PD-like disease in humans, can inhibit complex I of the respiratory chain (11). Some patients with pathogenic nuclear mutations that impair mtDNA stability also may develop a PD-like phenotype, showing that inherited mitochondrial dysfunction may be of importance in development of PD (12). In addition, genes found to be mutated in autosomal recessive forms of PD, e.g., Parkin and PTEN-induced putative kinase protein 1 (PINK1), also have been linked to regulation of mitochondrial function. Parkin and PINK1 have been shown to act in the same pathway, and loss of either gene in *Drosophila melanogaster* causes a degenerative phenotype with mitochondrial abnormalities (13–15). Mitochondrial impairment also has been reported in Parkin-knockout mice (16) but is not associated with cell loss (17).

Neurons depend on oxidative phosphorylation for energy supply and thus are vulnerable to mitochondrial compromise in vivo (18, 19). Neurons also have the unique requirement to maintain a functional pool of mitochondria at nerve endings far away from the cell nucleus (20). Mitochondrial biogenesis has been shown to take place in the perinuclear region (21), and mitochondria then are transported along microtubules to distal parts of axons and dendrites. Damaged mitochondria may be transported back to the soma for degradation or repair, but the mechanisms that ensure a healthy pool of mitochondria in the periphery remain unclear.

Recent studies in cell lines have shown that PINK1 and the ubiquitin ligase Parkin play a role in a pathway that selectively degrades impaired mitochondria (22–27). Exposure of cultured cells to toxins, e.g., carbonyl cyanide m-chlorophenylhydrazone (CCCP), which dissipates the mitochondrial membrane potential, leads to stabilization of the long isoform of PINK1 and recruitment of Parkin to the mitochondrial outer membrane. This recruitment leads to clustering of mitochondria in the perinuclear region and subsequent degradation by p62-mediated autophagy. Long-term forced expression of Parkin in a cell line also has been reported to promote selection against one, but not another, pathogenic heteroplasmic mtDNA mutation (28). These results have led to the hypothesis that the PINK1/Parkin pathway protects the mitochondrial network against accumulation of somatic mtDNA mutations. Age-associated decline of mitochondrial quality-control mechanisms may accelerate accumulation of somatic mtDNA mutations and be of central importance for the pathophysiology in sporadic PD also. However, such a unifying mechanism remains speculative at the moment, because Parkin-mediated selection against respiratory chain-deficient mitochondria remains to be demonstrated in vivo.

We studied the consequences of respiratory chain dysfunction on mitochondrial morphology and turnover in DA neurons in vivo using a reporter mouse for mitochondrial morphology. To model accumulation of mtDNA deletions in DA neurons, we used the MitoPark model with DA neuron-specific knockout of the gene for mitochondrial transcription factor A (*Tfam*) (19). TFAM is an essential protein that is an integral part of the basal transcription machinery for mtDNA and, in addition, also regulates mtDNA copy number by packaging and fully coating mtDNA (29). Loss of TFAM results in mtDNA depletion and abolishes mtDNA expression, causing severe respiratory chain deficiency (30). MitoPark mice appear healthy at birth but develop a slowly progressive degeneration of DA neurons as adults with depletion of striatal DA and impaired spontaneous locomotion (19, 31). Electron microscopy has shown that the degenerating DA neurons contain large intracellular, electron-

Author contributions: F.H.S., L.O., and N.-G.L. designed research; F.H.S., S.L., and R.W. performed research; F.H.S. contributed new reagents/analytic tools; F.H.S., L.O., and N.-G.L. analyzed data; and F.H.S., L.O., and N.-G.L. wrote the paper.

Conflict of interest statement: L.O. and N-G.L. are co-owners of Kampavata AB, which owns commercial rights to the MitoPark mouse.

This article is a PNAS Direct Submission.

[1]To whom correspondence should be addressed. Email: larsson@age.mpg.de.

This article contains supporting information online at www.pnas.org/lookup/suppl/doi:10.1073/pnas.1103295108/-/DCSupplemental.

NEUROSCIENCE

dense bodies that in part consist of a double-membrane structure resembling mitochondria. Using our reporter mouse, we report here that respiratory chain deficiency in DA neurons in vivo results both in mitochondrial fragmentation and formation of large mitochondrial aggregates. Although mitochondria in axon terminals are unaffected morphologically, the supply of mitochondria to striatal DA nerve terminals is decreased drastically because of impaired axonal transport. We also addressed the role of Parkin in mitochondrial quality control and found no evidence of Parkin recruitment to the defective mitochondria. In addition, knockout of Parkin has no effect on the formation of mitochondrial aggregates or progression of neurodegeneration.

Results

Generation of a Lox-Stop-Lox-Mito-YFP Reporter Mouse. To study mitochondrial morphology in vivo, we developed a reporter mouse with cell type-specific expression of YFP targeted to the mitochondrial matrix. A *lox*-flanked stop cassette was placed upstream of the mito-YFP transgene to restrict expression to cells in which the stop cassette has been removed by *cre*-mediated excision (Fig. 1*A* and Fig. S1*A*). The construct integrated by homologous recombination into the *Gt(ROSA)26Sor* locus (also called "ROSA26"), which has been used previously to create a number of reporter mice (32, 33). Targeted ES clones were identified by Southern blot analyses (Fig. S1*B*), and the allele was transmitted through the germline to create heterozygous *Gt(ROSA)26Sor*$^{+/lox\text{-}Stop\text{-}lox\text{-}mito\text{-}YFP}$ mice (herein called "ROSA26$^{+/SmY}$").

The stop cassette was removed in the germline by crossing ROSA26$^{+/SmY}$ mice to Actb-*cre* mice, which express *cre* from the β-actin promoter (Fig. S1*C*). The resulting mice had ubiquitous expression of mito-YFP and were healthy, with normal function of the respiratory chain (Fig. S2). These findings demonstrate that transgenic expression of mito-YFP does not interfere with mitochondrial function and thus can be used as a tool to study mitochondrial morphology in vivo.

Visualization of Mitochondria in DA Neurons. To study mitochondrial morphology in DA neurons, we crossed ROSA26$^{+/SmY}$ mice to DAT-*cre* mice that express *cre* under control of the DA transporter (Slc6a3) locus (19). The resulting offspring had undergone recombination specifically in the midbrain (Fig. 1*B*). Analysis of brain sections from these mice revealed robust expression of YFP specifically in DA-producing neurons in the SN pars compacta (SNc) and the ventral tegmental area of the midbrain (Fig. 1*C*). We counterstained mitochondria with an antibody against a translocase of the outer mitochondrial membrane (TOM20) and found by confocal microscopy that the signals overlap (Fig. 1*D*). Thus, our system allows faithful visualization of mitochondria in DA neurons in vivo.

The soma of DA neurons contained a dense network of tubular mitochondria (Fig. 2*A*, *Upper*). Mitochondria in proximal parts of axons and dendrites were elongated and often aligned side-by-side in parallel, whereas mitochondria further away from the soma were shorter and arranged along a single track. In striatum, labeled mitochondria typically were single, evenly distributed, and predominantly grain-like (Fig. 3*A* and Movie S1). The mitochondrial distribution and morphology in DA neurons thus appears similar to that described in cortical neurons but markedly different from that of lower motor neurons (34).

Mitochondrial Morphology in Respiratory Chain-Deficient DA Neurons. Next, we studied how mitochondrial morphology and distribution change in a situation of respiratory chain deficiency. We chose to monitor the mito-YFP expression pattern in DA neurons of MitoPark (genotype *Tfam*$^{loxP/loxP}$;DAT-*cre*; ROSA26$^{+/SmY}$) and control mice (genotype *Tfam*$^{+/+}$;DAT-*cre*; ROSA26$^{+/SmY}$). At early time points (age 4–8 wk), many MitoPark neurons contained one or more grossly enlarged, rounded mitochondria in the perinuclear region of the soma and in proximal segments of dendrites (Fig. 2*A*). In addition to these large, YFP^{+} mitochondrial aggregates, some cells also contained apparently fragmented mitochondria and in some cases multiple, small, spherical mitochondria clustered around the nucleus. The proportion of neurons with fragmented mitochondrial morphology increased with time (Fig. 2*B* and Fig. S3), and from 14 wk of age almost all DA neurons contained large mitochondrial-derived structures and had markedly shorter mitochondria in axons and dendrites. The enlarged mitochondria were immunoreactive to mitochondrial matrix protein superoxide dismutase 2 (SOD2) (Fig. 2*C*), whereas only the outer rim also was labeled with antibodies directed against the mitochondrial outer membrane protein TOM20 (Fig. 2*D*). This result shows that the large intracellular inclusions previously identified by light and electron microscopy in DA neurons of MitoPark mice indeed are of mitochondrial origin and that the enlargement depends on an increased matrix volume.

Maintained Morphology and Progressive Loss of Distal Axonal Mitochondria. The distal pool of mitochondria in striatal DA nerve fibers of MitoPark mice appeared surprisingly normal at age 8 wk (Fig. 3*A*). At later time points there were drastically fewer mitochondria, but no mitochondrial aggregates were found in striatum even at advanced disease stages. We analyzed the number and sizes of YFP-particles in dorsolateral striatum, the region of striatum in which the DA terminals first degenerate, and found a 45% reduction ($P < 0.01$) of mitochondrial numbers at 8 wk (Fig. 3*B*). This reduction affected all sizes equally (Fig. 3*C*). At 14 wk the loss of striatal mitochondria reached 88% ($P < 0.001$), and at this time point remaining mitochondria were slightly shifted toward increased size. We compared the loss of mitochondria to denervation by estimating the amount of tyrosine hydroxylase (TH)-positive fibers in the same areas. We

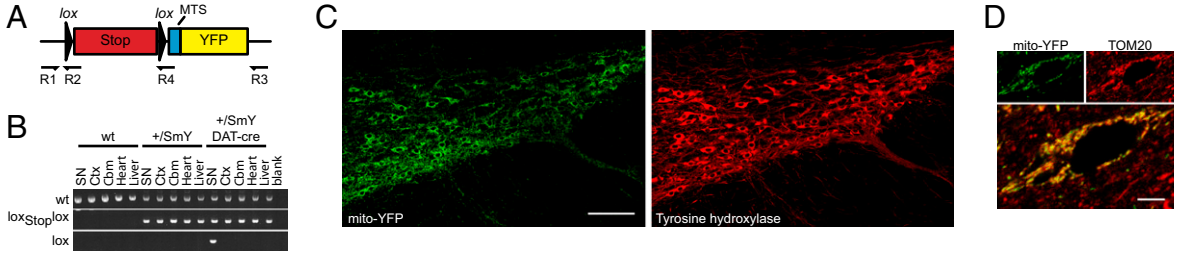

Fig. 1. Design of a lox-Stop-lox-mito-YFP cassette integrated into the ROSA26 locus and visualization of mitochondria in DA neurons. (*A*) Schematic illustration of the lox-Stop-lox-mito-YFP construct. The construct is driven by the endogenous ROSA26 promoter. MTS, mitochondrial targeting presequence lox, heterologous loxP-site lox2372 (Fig. S1). (*B*) Targeting (lox-Stop-lox) and recombination (lox) of the ROSA26 locus as detected by PCR in DNA from SN, cortex (Cx), cerebellum (Cbm), and heart and liver from wild-type ROSA26$^{+/SmY}$ and ROSA26$^{+/SmY}$;DAT-cre mice. (*C*) SNc DA neurons in a ROSA26$^{+/SmY}$;DAT-*cre* mouse. DA neurons are labeled with an antibody against TH. Quantification showed that 100% ($n = 388$) of SNc neurons that expressed YFP also were TH immunoreactive and that 99.5% ($n = 386$) of TH^{+} cells also expressed mito-YFP. (*D*) Confocal image of a neuron expressing mito-YFP (green) and labeled with an antibody against the mitochondrial protein TOM20 (red). (Scale bars: 100 μm in *C*; 5 μm in *D*.)

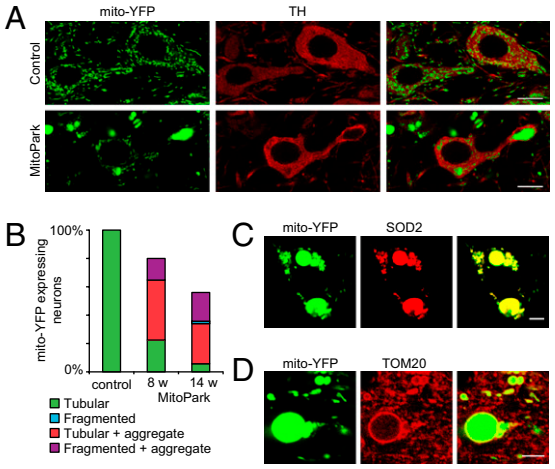

Fig. 2. Morphology of mitochondria in normal and respiratory chain-deficient DA neurons. (*A*) Confocal images of YFP-labeled mitochondria in DA neurons of 8-wk-old control (genotype *Tfam*$^{+/+}$;DAT-*cre*;ROSA26$^{+/SmY}$) and MitoPark (genotype *Tfam*$^{loxP/loxP}$;DAT-*cre*;ROSA26$^{+/SmY}$) mice. DA neurons also are identified by being TH immunoreactive (red). The detector gain of the YFP signal was decreased in the lower panel to prevent overexposure of the large aggregates. (*B*) Quantification of mitochondrial morphologies in neurons of control and MitoPark mice at 8 and 14 wk of age (Fig. S3). Data are normalized to the total numbers of cells counted separately. (*C*) MitoPark DA neuron expressing mito-YFP and labeled with an antibody against the mitochondrial matrix protein SOD2 (red). (*D*) Mitochondrial aggregates immunolabeled with an antibody against the mitochondrial outer membrane protein TOM20 (red). (Scale bar: 10 μm in *A*; 5 μm in *C* and *D*.)

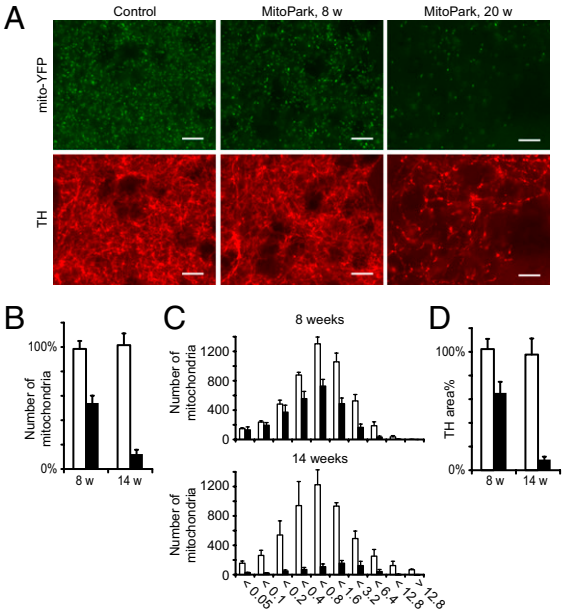

Fig. 3. Changes in the distal pool of mitochondria. (*A*) Epifluorescent images of mitochondria and dopaminergic fibers in striatum of control and MitoPark mice at age 8 and 20 wk. (Scale bars: 10 μm.) (*B*) Number of mitochondria in striatum of control and MitoPark mice at age 8 and 14 wk. (*C*) Size histograms showing volumes of YFP^{+} particles counted in *B*. (*D*) Denervation at 8 and 14 wk as measured by the area of optical sections occupied with TH-immunoreactive fibers. Open bars, controls; filled bars, MitoPark. Error bars indicate SEM. $n = 3$.

found a 36% reduction of TH density at 8 wk ($P < 0.05$) and a 91% reduction at 14 wk ($P < 0.01$) (Fig. 3*D*). Thus, the mitochondria in distal DA axons are spared morphologically and decline in numbers in parallel with the progressive degeneration of the nigrostriatal DA system.

Parkin Is Not Recruited to Dysfunctional Mitochondria. The current model holds that Parkin is recruited to dysfunctional mitochondria and facilitates their clearance, and we used our model to test this notion in vivo. We were unable to detect endogenous Parkin in DA neurons using immunocytochemistry, perhaps because of low expression levels. Instead, we used a strategy to overexpress Parkin fused to the fluorescent protein mCherry. Consistent with previous reports, we found that Cherry-Parkin translocates to mitochondria in transiently transfected HeLa cells upon exposure to CCCP (Fig. S4). We made adeno-associated virus (AAV) encoding Cherry-Parkin and delivered the construct to midbrain DA neurons of control and MitoPark mice by stereotactic injections. We found Parkin to have a cytoplasmic distribution (Fig. 4*A*), but we were unable to identify a single DA neuron in control or MitoPark mice where Parkin colocalized with mitochondria. Some neurons with strong expression displayed non-mitochondrial cytoplasmic dots, which possibly reflect protein aggregation associated with the overexpression.

Loss of Parkin Does Not Modify MitoPark Pathology. We hypothesized that absence of Parkin would prevent clearance of defective mitochondria and thereby worsen the pathology in MitoPark mice. To test this hypothesis, we generated MitoPark mice lacking Parkin expression (genotype *Tfam*$^{loxP/loxP}$;DAT-*cre*;Parkin$^{-/-}$). Loss of Parkin was confirmed by immunoblotting (Fig. S5*A*). Parkin-knockout MitoPark mice developed a phenotype indistinguishable from that of MitoPark mice with Parkin expression and showed impaired locomotion, rigidity, and weight loss from 20 wk of age. We proceeded to study mitochondrial morphology in MitoPark mice lacking Parkin (genotype *Tfam*$^{loxP/loxP}$;DAT-*cre*;Parkin$^{-/-}$;ROSA26$^{+/SmY}$) and found no effect on the formation of mitochondrial aggregates (Fig. 4 *B* and *C*). Likewise, mitochondria in the soma and striatum showed no significant differences in morphology or size (Fig. S5 *B* and *C*). We also investigated whether loss of Parkin had an effect on the progression of neurodegeneration by counting DA neurons in SNc of MitoPark mice with and without Parkin at age 30 wk (Fig. 4*D*). We found a similar degree of DA neuron loss in the SNc in MitoPark mice with and without Parkin expression (mean ± SEM 20.4 ± 2.8% and 22.5 ± 1.28%, respectively, compared with a control brain). Thus, Parkin is dispensable for the formation of large mitochondrial aggregates in vivo and does not modify the neurodegenerative process in MitoPark mice.

Import Competence of Enlarged Mitochondria. We studied the dynamics of mitochondrial biogenesis and transport in DA neurons of adult mice in vivo by delivery of a plasmid encoding dsRed fused to a mitochondrial leader peptide (mito-dsRed). We delivered viral particles by stereotactic injection into the SNc of MitoPark mice and controls with mito-YFP expression in their DA neurons. One week after viral injection a subset of the DA neurons and some other types of adjacent neurons showed robust expression of mito-dsRed. Transduced DA neurons were easy to identify as being double-labeled with mito-YFP and mito-dsRed. In control mice, there was a perfect overlap between the red and green fluorescence in the transduced DA neurons (Fig. 5*A*). Notably, the red fluorescence also accumulated in the large mitochondrial aggregates present in DA neurons of MitoPark neurons (Fig. 5*A*). Although the transduction efficiency of DA neurons of SNc 1 wk after injection was higher in control mice (mean ± SEM 45.6 ± 1.96%) than in MitoPark mice (34.2 ± 4.9%), the levels of mitochondrial red fluorescence were similar in DA neurons of control and MitoPark mice (Fig. 5*B*). However, the large mitochondrial aggregates in DA neurons of MitoPark mice showed significantly stronger red fluorescence than the small mitochondria present in DA neurons of either control or MitoPark mice (Fig. 5*B*). These results show that the

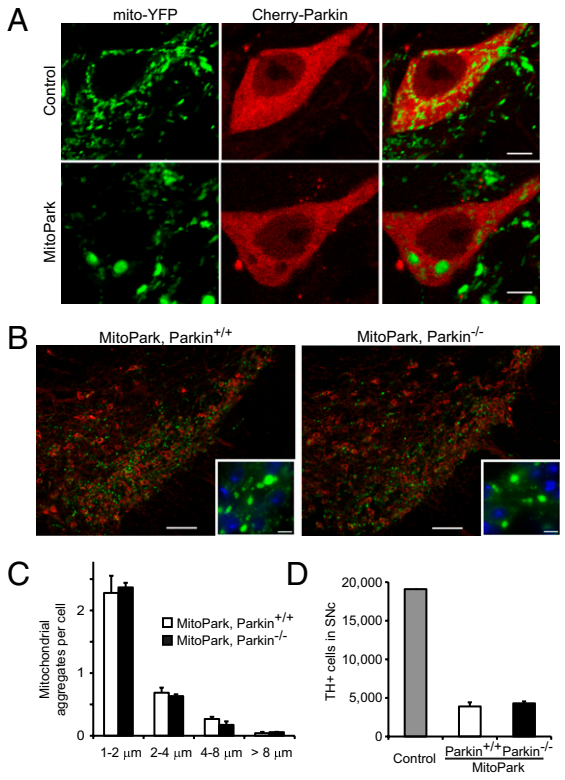

Fig. 4. Effect of Parkin on MitoPark pathology. (*A*) Control and MitoPark DA neurons expressing Cherry-Parkin 3 d after stereotactic viral delivery to the midbrain (age 7 wk). (Scale bars: 5 μm.) (*B*) Formation of large mitochondria-derived intracellular aggregates in midbrain DA neurons of 8-wk-old MitoPark mice with and without Parkin, respectively. YFP is shown in green, TH in red, and DAPI in blue. (Scale bars: 100 μm.) *Insets* show enlarged view. (Scale bars: 10 μm.) (*C*) Average number of enlarged mitochondria in the cell bodies of nigral DA neurons in MitoPark mice with and without Parkin (n = 3). (*D*) Stereological estimates of the number of TH-immunoreactive cells in bilateral SNc of ~30-w-old MitoPark mice with and without Parkin (n = 3).

abnormally enlarged mitochondria either retain the capacity to import mitochondrial proteins to the matrix, as supported by the observed expression of TOM20, or, alternatively, retain their capacity to fuse with small mitochondria that have previously imported mito-dsRed. Because both mitochondrial protein import and mitochondrial fusion require mitochondrial membrane potential, this finding provides indirect evidence for a preserved membrane potential in the enlarged mitochondria. Nevertheless, it was possible to identify rare cells (<1%) in which there was a clear discrepancy in the uptake of red fluorescent protein by smaller mitochondria and the largest aggregates (Fig. 5*C*), indicating that membrane potential of large mitochondrial aggregates may be lost eventually.

Supply of Distal Mitochondria Is Impaired. Next, we used the double-labeling strategy to address mitochondrial turnover in axon terminals. One week after viral delivery of mito-dsRed to SNc of 8-wk-old littermates, control mice were found to contain numerous double-labeled mitochondria (mito-YFP and mito-dsRed) in striatum, whereas strikingly fewer such double-labeled mitochondria were found in striatum of MitoPark mice (Fig. 5*D*). We counted the numbers of total (green only) and double-labeled (red and green) mitochondria in striatum and found that 20.2% of mitochondria were double labeled in control mice but only 1.5% were double labeled in MitoPark striatum (Fig. 5*E*). We normalized our numbers to compensate for the lower transduction efficiency and the DA neuron loss in MitoPark mice by dividing the total number of double-labeled mitochondria in striatum by the total number of double-labeled DA neurons for each injection (Fig. 5*F*). This normalization revealed an ~10-fold decrease in the number of fresh mitochondria in MitoPark striatum ($P < 0.001$). To exclude the possibility that this discrepancy was an effect of axon pathology, we studied retrograde axonal transport. After striatal injections of the retrograde tracer fluorogold (35), a similar proportion of SNc DA neurons were labeled in controls and MitoPark mice (Fig. 5*G* and Fig. S6*C*), demonstrating that the decreased supply of distal mitochondria was not caused by a focal block of axonal transport mechanisms (36). However, control neurons stained more intensely (Fig. S6*B*), suggesting impaired retrograde transport and/or uptake of fluorogold in axon terminals of MitoPark mice.

Discussion

We have shown that respiratory chain deficiency leads to the formation of grossly enlarged mitochondria in proximal parts of DA neurons in vivo. Depletion of mtDNA in skeletal muscle induces a compensatory increase in mitochondrial mass that helps maintain overall ATP production levels as the total number of poorly functioning mitochondria increases (37). Patients with mitochondrial dysfunction often have increased numbers of mitochondria, consistent with the idea that induction of mitochondrial biogenesis provides a compensatory response (38). Experimental induction of mitochondrial biogenesis can indeed ameliorate the severity of respiratory chain deficiency in skeletal muscle (39). It is possible that the large mitochondria formed in MitoPark neurons reflect a similar attempt to compensate loss of mitochondrial function by inducing mitochondrial biogenesis. However, such a response would be futile, because the anterograde transport of newly formed mitochondria to the distal parts of the axons is impaired severely. It is not clear whether this transport defect is a direct consequence of ATP deficiency, failure to form transportable units, or clogging of the neural processes. The large mitochondria in MitoPark neurons probably are not products of excessive fusion, because there is concurrent mitochondrial fragmentation, consistent with previous reports of mitochondrial fragmentation in cells and tissues with respiratory chain deficiency (40). Also, the large, pathological, mitochondria-derived aggregates seem unable to pass the axon hillock, because they are found only in the perikaryon and in proximal dendrites but never in DA target areas of MitoPark mice. Mice that lack the mitochondrial fission protein Dynamin-related protein 1 also form enlarged mitochondria and fail to distribute mitochondria for proper synapse formation (41), thus demonstrating the importance of proper regulation of mitochondrial size in the maintenance of synapses. In MitoPark mice, loss of dopaminergic innervation of striatum precedes the loss of DA neuron cell bodies in the midbrain by weeks to months, and depletion of functional mitochondria in the axons may explain this "dying-back" degeneration.

Mitochondria undergo continuous fission and fusion (42), and it has been shown in cell culture systems that mitochondria with a lower membrane potential are isolated by impaired fusion (43) and labeled by Parkin for selective degradation (22). Such continual functional testing of the mitochondrial network would provide a quality-control mechanism whereby mitochondria with damaged respiratory chain function are removed. We have addressed the role of Parkin in vivo in mice with progressive respiratory chain failure in DA neurons caused by loss of mtDNA expression. Respiratory chain-deficient DA neurons develop large mitochondria-derived aggregates resembling those seen in cells exposed to CCCP (25), but we found no evidence of Parkin recruitment to mitochondria. ATP deficiency has been suggested to explain, at least in part, why Parkin translocation could not be detected in CCCP-treated primary neurons (44). The neurodegeneration in MitoPark mice progresses over the course of 30–40 wk, and there is heterogeneity of mitochondrial morphology even within a single cell, suggesting that ATP deficiency is less drastic than in cells acutely depolarized by CCCP. Another possibility is that the impaired mitochondria in Mito-

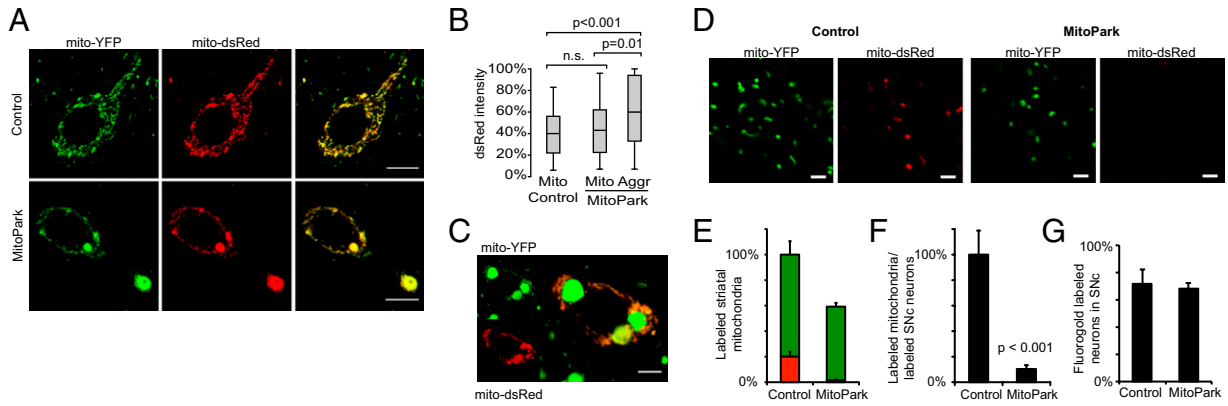

Fig. 5. Uptake and axonal transport of mitochondrial red fluorescent protein. (*A*) Confocal images of double-labeled control and MitoPark neurons that express both mito-YFP and mito-dsRed 1 wk after stereotactic injections of AAV-mito-dsRed to the SNc. Mice were analyzed at age 8 wk. (*B*) Box plots showing dsRed intensities in small mitochondria and large mitochondria-derived aggregates (Aggr) in transduced control and MitoPark neurons ($n \geq 37$ cells). Mice were analyzed at age 8 wk. (*C*) Example of a MitoPark neuron with heterogeneous uptake of mito-dsRed 1 wk after viral delivery. The YFP signal from the enlarged mitochondria was saturated to allow visualization of smaller mitochondria. (*D*) High-magnification image of striatal areas with mitochondria that contain YFP and dsRed. (*E*) Quantification of YFP-labeled mitochondria (green bar) and YFP-labeled mitochondria that also contain dsRed (red bar) in striatum of MitoPark mice and controls 1 wk after viral delivery to the SNc. Percentages relate to the number of mitochondria counted in controls (3,137). (*F*) Number of double-labeled striatal mitochondria normalized by the number of double-labeled SNc neurons ($n = 6$). (*G*) Proportion of mito-YFP$^+$, fluorogold–labeled SNc neurons in 8-wk-old mice 48 h after striatal injections of fluorogold ($n = 4$). (Scale bars: 10 μm in *A*; 5 μm in *C*; 2 μm in *D*.)

Park mice maintain a membrane potential above the threshold needed for Parkin recruitment. Cultured cells completely lacking mtDNA (ρ^0 cells) have the capacity to maintain the mitochondrial membrane potential because of the activity of an F_1–ATPase subcomplex (45, 46), and Parkin translocation in ρ^0 cells is increased if the F_1–ATPase subcomplex is inhibited (28). Similarly, mitochondria in DA neurons of MitoPark mice probably maintain a mitochondrial membrane potential, as suggested by the finding that even very enlarged mitochondria can import proteins to the mitochondrial matrix. Our results emphasize important differences between the severe decrease in membrane potential caused by acute exposure to depolarizing toxins in vitro and the slow deterioration of mitochondrial function observed in mitochondrial disease in vivo. There is strong selection against deleterious mtDNA mutations in the female germ line (47, 48), but there is no solid evidence for negative selection against mutated mtDNA in postmitotic tissues of patients with pathogenic mtDNA mutations (49). On the contrary, there are some reports showing that the fraction of mutated mtDNA actually may increase over time in patients with mitochondrial diseases (50). Our results suggest that Parkin-mediated mitophagy is a rare event in vivo and that the loss of membrane potential caused by the loss of mtDNA is insufficient to allow Parkin to select against mtDNA deletions. Instead, we speculate that Parkin-mediated autophagy acts as a mechanism to protect the mitochondrial network against mitochondria that have complete or nearly complete loss of membrane potential. Fusion of a depolarized mitochondrion can propagate the depolarization to the rest of the mitochondrial network, and mechanisms that prevent such a deleterious event would be of particular importance in postmitotic cells such as neurons. Finally, loss of Parkin may cause Parkinsonism by pathways other than impaired quality control, as exemplified by a recent publication in which Parkin was found to regulate mitochondrial biogenesis through peroxisome proliferator-activated receptor γ coactivator 1-α by degrading the transcriptional repressor Zinc finger protein 746 (PARIS) (51).

In summary, we present a reporter mouse that allows specific studies of mitochondrial structure and dynamics in normal and degenerating DA neurons, including their axon terminals. We use this model to demonstrate that severe respiratory chain dysfunction in DA neurons leads to fragmentation of the mitochondrial network, formation of large mitochondrial aggregates, and an impaired supply of fresh mitochondria to DA nerve terminals in striatum. In addition, we present findings that do not support a model in which Parkin-induced mitophagy protects against accumulation of mitochondria with severe respiratory chain dysfunction in vivo, because dysfunctional mitochondria do not recruit Parkin and because neither clearance of defective mitochondria nor the neurodegeneration phenotype is affected by the absence of Parkin. Taken together, these observations have implications for understanding the pathophysiology in several different types of mitochondrial neurodegeneration.

Materials and Methods

Details about the breeding and handling of mice, Southern and Western blot, biochemical measurements, tissue processing, immunohistochemistry, stereology, stereotactic injections, cell culture, and statistical analysis are given in *SI Materials and Methods*.

Generation of Lox-Stop-Lox-Mito-YFP Mice. A plasmid containing 5′-NheI-splice acceptor-loxP-polyA-polyA-FRT-Neo-FRT-Westfal Stop cassette-loxP-EcoRV-GFP-EcoRV-NheI-3′ was obtained (52). The Westphal stop cassette contains two polyA sequences in tandem and a false translation initiation site followed by a splice donor that efficiently inhibits transcription and translation of downstream genes. To minimize interference with wild-type loxP sites in *trans*, the 5′ and 3′ loxP sites were mutated to heterologous lox2372 sites (ataacttcgtataggatacttatacgaagttat) (53) by PCR and by replacement with a synthetic linker, respectively. Next, the EcoRV-GFP-EcoRV fragment was replaced with a KpnI-SmaI linker. This linker was used to introduce the cDNA of YFP fused at its N terminus with the mitochondrial targeting presequence of the mitochondrial matrix protein ornithine transcarbamylase. The transgene cassette was excised with NheI and introduced into the XbaI site of a ROSA26 targeting vector. The targeting vector was linearized and electroporated into 129R1 ES cells. Targeted clones were identified by Southern blot analysis. Positive clones were used for blastocyst injection, and germ line transmission was obtained by mating chimeric mice to C57BL/6 mice.

Microscopy. Epifluorescent images were acquired using a DMI6000 microscope (Leica) using 10×/0.3 NA or 40×/0.6 NA dry objectives and filter cubes A4 (360/40; 400; 470/40) for DAPI, YFP (500/20; 515; 535/30) for YFP, and N2.1 (515-560; 580; LP590) for Cy3. Confocal images were acquired by sequential scanning using a LSM510 Meta microscope (Zeiss). YFP was excited with the 514-nm argon laser and emission was detected at 520–542 nm. Cy3, mCherry, and dsRed were excited with 543-nm helium-neon laser and detected at 553–649 nm, 584–638 nm, and 595–659 nm, respectively.

Image Analysis and Quantifications. Image analysis was performed using ImageJ. For quantifications of striatal mitochondria, confocal images were acquired from systematically selected areas in dorsolateral parts of striatum

in coronary brain sections (0.2–1 mm anterior to bregma). Three areas were acquired per section, and three sections per brain were analyzed. Striatal volume stacks of 40 × 40 × 10 μm were acquired using a 100×/1.45 NA oil objective. Images were noise-reduced by a median filter (*despeckle*), binarized, and the number and volume of YFP^+ particles (diameter >0.3 μm) were counted using the ObjectCounter3D ImageJ plug-in. TH density was estimated by measuring the area of the fractions of binarized optical sections that were TH immunoreactive. Numbers of YFP^- and YFP^+dsRed^+ particles in striatum were counted using the ImageJ *Analyze particles* algorithm in optical sections (105 μm × 105 μm × <2.0 μm) acquired using a 40×/1.3 NA oil objective. For measurements of dsRed intensities, transduced cells were imaged with an optical section thickness <0.5 μm using a 100×/1.45 NA oil objective.

Generation of AAV Vectors. A sequence encoding a fusion protein of the red fluorescent protein dsRed1 fused to the mitochondrial targeting sequence from subunit VIII of human cytochrome *c* oxidase (pDsRed1-Mito; Clontech) was inserted in the XbaI site of pAAV-MCS, a vector that contains a CMV promoter and a β-globin intron and is flanked by two AAV inverted terminal repeats. Mouse Parkin was amplified from a cDNA clone (Imagene) by PCR. The resulting SalI-Parkin-HindIII fragment was sequenced and inserted in pAAV-MCS, and subsequently a NheI-mCherry-SalI fragment (Clontech) was inserted upstream. The constructs in the pAAV vectors were packaged into AAV2/1 by large-scale transfection of HEK293 cells, and viral particles were purified by serial $CsCl_2$ centrifugation (Vector Biolabs).

ACKNOWLEDGMENTS. We thank Karin Lundströmer and Karin Pernold for technical assistance, Dr. Ari Waisman for providing the plasmid containing the stop cassette, Dr. Philippe Soriano for providing the ROSA26-targeting vector, and A. Brice for the Parkin knockout mice. This work is supported by the National Institutes of Health-Karolinska Institute Graduate Partnership Program for the Neurosciences, Grants K2011-62X-21870-01-6 and K2009-61X-03185-39-3 from the Swedish Research Council, Swedish Brain Power, the Parkinson Foundation, and Karolinska Institute.

1. Krishnan KJ, Greaves LC, Reeve AK, Turnbull D (2007) The ageing mitochondrial genome. *Nucleic Acids Res* 35:7399–7405.
2. Larsson NG (2010) Somatic mitochondrial DNA mutations in mammalian aging. *Annu Rev Biochem* 79:683–706.
3. Müller-Höcker J (1989) Cytochrome-c-oxidase deficient cardiomyocytes in the human heart—an age-related phenomenon. A histochemical ultracytochemical study. *Am J Pathol* 134:1167–1173.
4. Bua E, et al. (2006) Mitochondrial DNA-deletion mutations accumulate intracellularly to detrimental levels in aged human skeletal muscle fibers. *Am J Hum Genet* 79: 469–480.
5. Taylor RW, et al. (2003) Mitochondrial DNA mutations in human colonic crypt stem cells. *J Clin Invest* 112:1351–1360.
6. Cottrell DA, et al. (2001) Cytochrome c oxidase deficient cells accumulate in the hippocampus and choroid plexus with age. *Neurobiol Aging* 22:265–272.
7. Bender A, et al. (2006) High levels of mitochondrial DNA deletions in substantia nigra neurons in aging and Parkinson disease. *Nat Genet* 38:515–517.
8. Corral-Debrinski M, et al. (1992) Mitochondrial DNA deletions in human brain: Regional variability and increase with advanced age. *Nat Genet* 2:324–329.
9. Soong NW, Hinton DR, Cortopassi G, Arnheim N (1992) Mosaicism for a specific somatic mitochondrial DNA mutation in adult human brain. *Nat Genet* 2:318–323.
10. Bender A, et al. (2008) Dopaminergic midbrain neurons are the prime target for mitochondrial DNA deletions. *J Neurol* 255:1231–1235.
11. Smeyne RJ, Jackson-Lewis V (2005) The MPTP model of Parkinson's disease. *Brain Res Mol Brain Res* 134:57–66.
12. Luoma P, et al. (2004) Parkinsonism, premature menopause, and mitochondrial DNA polymerase gamma mutations: Clinical and molecular genetic study. *Lancet* 364: 875–882.
13. Clark IE, et al. (2006) Drosophila pink1 is required for mitochondrial function and interacts genetically with parkin. *Nature* 441:1162–1166.
14. Park J, et al. (2006) Mitochondrial dysfunction in Drosophila PINK1 mutants is complemented by parkin. *Nature* 441:1157–1161.
15. Yang Y, et al. (2006) Mitochondrial pathology and muscle and dopaminergic neuron degeneration caused by inactivation of Drosophila Pink1 is rescued by Parkin. *Proc Natl Acad Sci USA* 103:10793–10798.
16. Palacino JJ, et al. (2004) Mitochondrial dysfunction and oxidative damage in parkin-deficient mice. *J Biol Chem* 279:18614–18622.
17. Itier JM, et al. (2003) Parkin gene inactivation alters behaviour and dopamine neurotransmission in the mouse. *Hum Mol Genet* 12:2277–2291.
18. Sörensen L, et al. (2001) Late-onset corticohippocampal neurodepletion attributable to catastrophic failure of oxidative phosphorylation in MILON mice. *J Neurosci* 21: 8082–8090.
19. Ekstrand MI, et al. (2007) Progressive parkinsonism in mice with respiratory-chain-deficient dopamine neurons. *Proc Natl Acad Sci USA* 104:1325–1330.
20. MacAskill AF, Kittler JT (2010) Control of mitochondrial transport and localization in neurons. *Trends Cell Biol* 20:102–112.
21. Davis AF, Clayton DA (1996) In situ localization of mitochondrial DNA replication in intact mammalian cells. *J Cell Biol* 135:883–893.
22. Narendra D, Tanaka A, Suen DF, Youle RJ (2008) Parkin is recruited selectively to impaired mitochondria and promotes their autophagy. *J Cell Biol* 183:795–803.
23. Narendra DP, et al. (2010) PINK1 is selectively stabilized on impaired mitochondria to activate Parkin. *PLoS Biol* 8:e1000298.
24. Matsuda N, et al. (2010) PINK1 stabilized by mitochondrial depolarization recruits Parkin to damaged mitochondria and activates latent Parkin for mitophagy. *J Cell Biol* 189:211–221.
25. Lee JY, Nagano Y, Taylor JP, Lim KL, Yao TP (2010) Disease-causing mutations in parkin impair mitochondrial ubiquitination, aggregation, and HDAC6-dependent mitophagy. *J Cell Biol* 189:671–679.
26. Geisler S, et al. (2010) PINK1/Parkin-mediated mitophagy is dependent on VDAC1 and p62/SQSTM1. *Nat Cell Biol* 12:119–131.
27. Vives-Bauza C, et al. (2010) PINK1-dependent recruitment of Parkin to mitochondria in mitophagy. *Proc Natl Acad Sci USA* 107:378–383.
28. Suen DF, Narendra DP, Tanaka A, Manfredi G, Youle RJ (2010) Parkin overexpression selects against a deleterious mtDNA mutation in heteroplasmic cybrid cells. *Proc Natl Acad Sci USA* 107:11835–11840.
29. Falkenberg M, Larsson NG, Gustafsson CM (2007) DNA replication and transcription in mammalian mitochondria. *Annu Rev Biochem* 76:679–699.
30. Larsson NG, et al. (1998) Mitochondrial transcription factor A is necessary for mtDNA maintenance and embryogenesis in mice. *Nat Genet* 18:231–236.
31. Galter D, et al. (2010) MitoPark mice mirror the slow progression of key symptoms and L-DOPA response in Parkinson's disease. *Genes Brain Behav* 9:173–181.
32. Mao X, Fujiwara Y, Orkin SH (1999) Improved reporter strain for monitoring Cre recombinase-mediated DNA excisions in mice. *Proc Natl Acad Sci USA* 96:5037–5042.
33. Soriano P (1999) Generalized lacZ expression with the ROSA26 Cre reporter strain. *Nat Genet* 21:70–71.
34. Misgeld T, Kerschensteiner M, Bareyre FM, Burgess RW, Lichtman JW (2007) Imaging axonal transport of mitochondria in vivo. *Nat Methods* 4:559–561.
35. Schmued LC, Fallon JH (1986) Fluoro-Gold: A new fluorescent retrograde axonal tracer with numerous unique properties. *Brain Res* 377:147–154.
36. Coleman M (2005) Axon degeneration mechanisms: Commonality amid diversity. *Nat Rev Neurosci* 6:889–898.
37. Wredenberg A, et al. (2002) Increased mitochondrial mass in mitochondrial myopathy mice. *Proc Natl Acad Sci USA* 99:15066–15071.
38. Smeitink JA, Zeviani M, Turnbull DM, Jacobs HT (2006) Mitochondrial medicine: A metabolic perspective on the pathology of oxidative phosphorylation disorders. *Cell Metab* 3:9–13.
39. Wenz T, Diaz F, Spiegelman BM, Moraes CT (2008) Activation of the PPAR/PGC-1alpha pathway prevents a bioenergetic deficit and effectively improves a mitochondrial myopathy phenotype. *Cell Metab* 8:249–256.
40. Duvezin-Caubet S, et al. (2006) Proteolytic processing of OPA1 links mitochondrial dysfunction to alterations in mitochondrial morphology. *J Biol Chem* 281: 37972–37979.
41. Ishihara N, et al. (2009) Mitochondrial fission factor Drp1 is essential for embryonic development and synapse formation in mice. *Nat Cell Biol* 11:958–966.
42. Hoppins S, Lackner L, Nunnari J (2007) The machines that divide and fuse mitochondria. *Annu Rev Biochem* 76:751–780.
43. Twig G, et al. (2008) Fission and selective fusion govern mitochondrial segregation and elimination by autophagy. *EMBO J* 27:433–446.
44. Van Laar VS, et al. (2011) Bioenergetics of neurons inhibit the translocation response of Parkin following rapid mitochondrial depolarization. *Hum Mol Genet* 20:927–940.
45. Appleby RD, et al. (1999) Quantitation and origin of the mitochondrial membrane potential in human cells lacking mitochondrial DNA. *Eur J Biochem* 262:108–116.
46. Buchet K, Godinot C (1998) Functional F1-ATPase essential in maintaining growth and membrane potential of human mitochondrial DNA-depleted rho degrees cells. *J Biol Chem* 273:22983–22989.
47. Stewart JB, Freyer C, Elson JL, Larsson NG (2008) Purifying selection of mtDNA and its implications for understanding evolution and mitochondrial disease. *Nat Rev Genet* 9:657–662.
48. Stewart JB, et al. (2008) Strong purifying selection in transmission of mammalian mitochondrial DNA. *PLoS Biol* 6:e10.
49. Chinnery PF, Samuels DC, Elson J, Turnbull DM (2002) Accumulation of mitochondrial DNA mutations in ageing, cancer, and mitochondrial disease: Is there a common mechanism? *Lancet* 360:1323–1325.
50. Larsson NG, Holme E, Kristiansson B, Oldfors A, Tulinius M (1990) Progressive increase of the mutated mitochondrial DNA fraction in Kearns-Sayre syndrome. *Pediatr Res* 28: 131–136.
51. Shin JH, et al. (2011) PARIS (ZNF746) repression of PGC-1α contributes to neurodegeneration in Parkinson's disease. *Cell* 144:689–702.
52. Buch T, et al. (2005) A Cre-inducible diphtheria toxin receptor mediates cell lineage ablation after toxin administration. *Nat Methods* 2:419–426.
53. Siegel RW, Jain R, Bradbury A (2001) Using an in vivo phagemid system to identify non-compatible loxP sequences. *FEBS Lett* 505:467–473.